# Mechanically Activated Combustion Synthesis of $MoSi_2$-Based Composites

Final Scientific/Technical Report

| | |
|---|---|
| Reporting Period Start Date: | July 1, 2012 |
| Reporting Period End Date: | September 30, 2015 |
| Principal Author: | Dr. Evgeny Shafirovich |
| Date Report was Issued: | December 2015 |
| DOE Award Number: | DE-FE0008470 |
| Name and Address of Submitting Organization: | The University of Texas at El Paso<br>500 W. University Ave., El Paso, TX 79968 |

## Disclaimer

## Abstract

The thermal efficiency of gas-turbine power plants could be dramatically increased by the development of new structural materials based on molybdenum silicides and borosilicides, which can operate at temperatures higher than 1300 °C with no need for cooling. A major challenge, however, is to simultaneously achieve high oxidation resistance and acceptable mechanical properties at high temperatures. One approach is based on the fabrication of $MoSi_2$–$Mo_5Si_3$ composites that combine high oxidation resistance of $MoSi_2$ and good mechanical properties of $Mo_5Si_3$. Another approach involves the addition of boron to Mo-rich silicides for improving their oxidation resistance through the formation of a borosilicate surface layer. In particular, materials based on $Mo_5SiB_2$ phase are promising materials that offer favorable combinations of high temperature mechanical properties and oxidation resistance. However, the synthesis of Mo–Si–B multi-phase alloys is difficult because of their extremely high melting temperatures. Mechanical alloying has been considered as a promising method, but it requires long milling times, leading to large energy consumption and contamination of the product by grinding media.

In the reported work, $MoSi_2$–$Mo_5Si_3$ composites and several materials based on $Mo_5SiB_2$ phase have been obtained by mechanically activated self-propagating high-temperature synthesis (MASHS). Short-term milling of Mo/Si mixture in a planetary mill has enabled a self-sustained propagation of the combustion front over the mixture pellet, leading to the formation of $MoSi_2$–$T_1$ composites. Combustion of Mo/Si/B mixtures for the formation of $T_2$ phase becomes possible if the composition is designed for the addition of more exothermic reactions leading to the formation of MoB, TiC, or $TiB_2$. Upon ignition, Mo/Si/B and Mo/Si/B/Ti mixtures exhibited spin combustion, but the products were porous, contained undesired secondary phases, and had low oxidation resistance. It has been shown that use of SHS compaction (quasi-isostatic pressing after combustion) significantly improves oxidation resistance of the obtained $MoSi_2$–$Mo_5Si_3$ composites. The “chemical oven” technique has been successfully employed to fabricate low-porous $Mo_5SiB_2$–TiC, $Mo_5SiB_2$–$TiB_2$, and Mo–$Mo_5SiB_2$–$Mo_3Si$ materials. Among them, $Mo_5SiB_2$–$TiB_2$ material possesses good mechanical properties and simultaneously exhibits excellent oxidation resistance at temperatures up to 1500 °C.

# Table of Contents

# 1. Executive Summary

The thermal efficiency of gas-turbine power plants could be dramatically increased by the development of new structural materials based on molybdenum silicides and borosilicides, which can operate at temperatures higher than 1300 °C with no need for cooling [1-4]. A major challenge, however, is to simultaneously achieve high oxidation resistance and acceptable mechanical properties at high temperatures. For example, molybdenum disilicide ($MoSi_2$) has excellent oxidation resistance and poor mechanical properties, while Mo-rich silicides such as $Mo_5Si_3$ (called $T_1$) have much better mechanical properties but poor oxidation resistance [4, 5].

One approach is based on the fabrication of $MoSi_2$−$T_1$ composites that combine high oxidation resistance of $MoSi_2$ and good mechanical properties of $T_1$. Another approach involves the addition of boron to Mo-rich silicides for improving their oxidation resistance through the formation of a borosilicate surface layer [1, 6]. In particular, $Mo_5SiB_2$ (called $T_2$) phase is considered as an attractive material. Boron addition, however, makes silicides brittle. One way to toughen these mixtures is to add molybdenum phase. Three-phase α-Mo–$Mo_5SiB_2$–$Mo_3Si$ (e.g., Mo–12Si–8.5B) alloys are considered as promising materials that combine good oxidation resistance and acceptable mechanical properties [7-9]. A novel method for improving the mechanical properties of $Mo_5SiB_2$ materials involves the addition of titanium carbide (TiC) [10, 11]. One more potential additive to $T_2$ phase is titanium diboride ($TiB_2$). However, to the best of our knowledge, no attempt has been made to fabricate $Mo_5SiB_2$–$TiB_2$ materials.

The synthesis of Mo−Si−B multi-phase alloys is usually difficult because of their extremely high melting temperatures. Mechanical alloying has been considered as a promising method for manufacturing these materials [9, 12, 13]. This method, however, requires long milling times, leading to large energy consumption and contamination of the product by grinding media.

The goal of the project was to develop a novel and competitive processing route for manufacturing $MoSi_2$- and $Mo_5SiB_2$-based composites. Specifically, the project has investigated use of mechanically activated self-propagating high-temperature synthesis (MASHS), a relatively low-cost and fast technique [14, 15].

The research objectives included determination of optimal MASHS conditions for production of $MoSi_2$ and $Mo_5SiB_2$ ($T_2$ phase) reinforced with secondary phases, development of an SHS compaction technique for densification of these composites obtained by MASHS, and determination of mechanical and oxidation properties of these composites produced by MASHS-compaction.

In the reported work, $MoSi_2$−$T_1$ composites and several materials based on $T_2$ phase have been obtained by MASHS. Short-term milling of Mo-Si mixture in a planetary mill has enabled a self-sustained propagation of the combustion front over the mixture pellet, leading to the formation of $MoSi_2$−$T_1$ composites.

It has been demonstrated that a self-sustained combustion of Mo/Si/B mixtures for the formation of $T_2$ phase becomes possible if the composition is designed for the addition of more exothermic reactions leading to the formation of MoB, TiC, or $TiB_2$. Upon ignition, Mo/Si/B and Mo/Si/B/Ti

mixtures exhibited a self-sustained propagation of a spinning combustion wave, but the products were porous, contained undesired secondary phases, and had low oxidation resistance. Two approaches have been tested for the fabrication of denser materials. One approach is the so-called SHS compaction, where the mixture burns in a special die under a uniaxial hydraulic press and is subjected to quasi-isostatic pressing immediately after combustion. It has been shown that SHS compaction significantly improves oxidation resistance of the obtained $MoSi_2$–$T_1$ composites.

Another tested approach is the so-called "chemical oven" technique, which involves composite pellets consisting of a core of the main mixture and a shell of highly exothermic mixture such as Ti/B. This technique has been successfully employed to fabricate low-porous $Mo_5SiB_2$–TiC, $Mo_5SiB_2$–$TiB_2$, and Mo–$Mo_5SiB_2$–$Mo_3Si$ materials. Among them, $Mo_5SiB_2$–$TiB_2$ material possesses good mechanical properties and simultaneously exhibits excellent oxidation resistance at temperatures up to 1500 °C.

*In summary, the research has shown that mechanically activated combustion synthesis can be successfully used for the fabrication of $MoSi_2$–$Mo_5Si_3$ composites and materials based on $Mo_5SiB_2$ phase. For the first time, $Mo_5SiB_2$–$TiB_2$ material has been synthesized. This material, obtained by the chemical oven technique, has good mechanical properties and excellent oxidation resistance at temperatures up to 1500 °C.*

# 2. Report Details

## 2.1. Experimental Methods

Molybdenum (99.95% pure, Climax Molybdenum), silicon (crystalline, 99.5% pure, Alfa Aesar), boron (amorphous, 94–96% pure, Alfa Aesar), graphite (crystalline, 99% pure, Alfa Aesar), and titanium (99.5% pure, Alfa Aesar) powders were used in this study.

Particle size distributions for these powders were determined with a multi-laser particle size analyzer (Microtrac Bluewave).

The powders were mixed in a three-dimensional inversion kinematics tumbler mixer (Inversina 2L, from Bioengineering, Inc.) for 1 h and then milled in a planetary ball mill (Fritsch Pulverisette 7 premium line). Zirconia-coated 80-mL bowls were used. The grinding media were 1.5-mm zirconia balls. The mixture to ball mass ratio was equal to 1:6. The milling process included 4 milling-cooling cycles (10 min milling at the maximum rotation speed of 1100 rpm and 75 min cooling).

To obtain $MoSi_2$-$Mo_5Si_3$ composite, a mixture of 38.87 mol% Mo and 61.13 mol% Si was prepared. This mixture corresponds to the expected product composition 80 vol% $MoSi_2$ and 20 vol% $Mo_5Si_3$ (91.92 mol% $MoSi_2$ and 8.08 mol% $Mo_5Si_3$). The as-milled powders were compacted into cylindrical pellets in a uniaxial hydraulic press (Carver; force: 10–40 kN). Before compacting, a layer of Ti/B (1:2 mole ratio) booster mixture was placed on the top of the pellet. The pellet diameter was 13 mm in most experiments. Some SHS compaction tests were also conducted with 25-mm diameter pellets. The pellet height was 20–25 mm. The relative density of the pressed samples was 55–60 %.

To fabricate $Mo_5SiB_2$–TiC materials by conventional SHS (with no external heat), four compositions were tested. Different amounts (10 wt%, 20 wt%, 30 wt%, and 40%) of stoichiometric Ti/C (1:1 mole ratio) mixture were added to the main Mo/Si/B (5:1:2 mole ratio) mixture. To fabricate $Mo_5SiB_2$–$TiB_2$ materials by the same technique, five compositions were tested. Different amounts (10 wt%, 15 wt%, 20 wt%, 30 wt%, and 40 wt%) of stoichiometric Ti-B (1:2 mole ratio) mixture were added to Mo/Si/B (5:1:2 mole ratio) mixture. The resulting mixtures were compressed into cylindrical pellets (diameter 13 mm) in the hydraulic press with a compressive force of 35-40 kN. Before compacting, a layer of Ti/B (1:2 mole ratio) booster mixture was placed on the top of the pellet. The height of the main mixture was 12-15 mm and the height of the booster layer was about 3 mm. The relative densities of the tested mixtures were in the range of 57–66 %.

In the chemical oven technique, composite pellets were prepared that included a core made of the main mixture and a shell made of the Ti/B booster mixture. The core compositions for fabricating $Mo_5SiB_2$–TiC and $Mo_5SiB_2$–$TiB_2$ materials consisted of 85 wt% Mo/Si/B (5:1:2 mole ratio) mixture and 15 wt% Ti/B (1:2 mole ratio) or Ti/C (1:1 mole ratio) mixture. The core compositions for fabricating α-Mo–$Mo_5SiB_2$–$Mo_3Si$ materials consisted of Mo, Si, and B mixed according to the composition of Mo–12Si–8.5B alloy. To make the composite pellet, first, the core mixture was compacted into a pellet (diameter: 13 mm, height: 12.8−14.0 mm) using a force

of 35-40 kN. Then this pellet was submerged into Ti/B mixture inside a 25-mm die and pressed again. The resulting composite pellet had a height of 23-26 mm. This pellet was wrapped by 3-mm-thick thermal paper (Fiberfrax). Figure 1 shows sketches of pellets prepared for conventional SHS and chemical oven experiments.

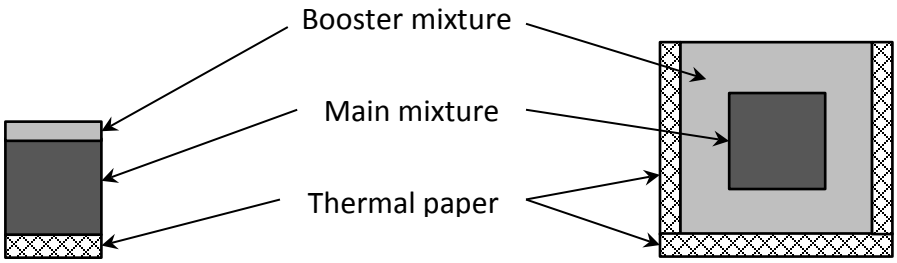


**Fig. 1. Sketches of pellets prepared for conventional SHS (left) and chemical oven experiments (right).**

The combustion experiments were conducted in a 30-L stainless steel reaction chamber. Figure 2 shows a schematic diagram of the setup. The pellet was installed vertically on a ceramic fiber insulator (Fiberfrax). The chamber was evacuated and filled with ultrahigh purity argon at 1 atm. The pellet was heated by a tungsten wire connected to a DC power supply. During conventional SHS, propagation of the combustion front over the pellet was observed, while in the chemical oven experiments, it was possible to only see bright light emitted by the burning shell. In both types of experiments, the power supply was shut off upon the ignition of the booster mixture.

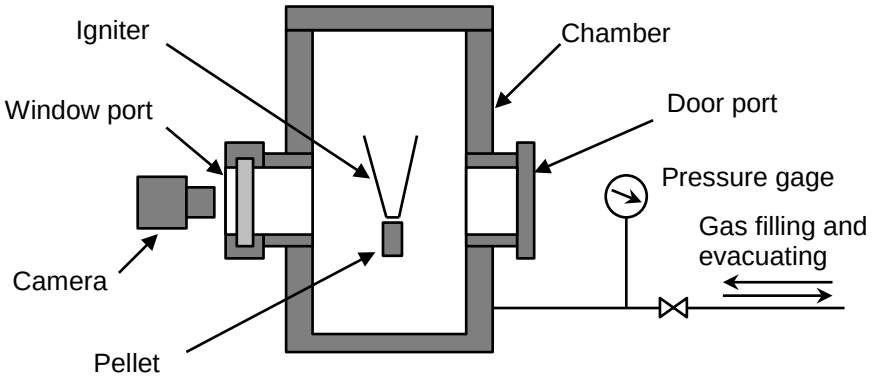


**Fig. 2. Schematic diagram of the reaction chamber.**

A steel die for SHS compaction has an inner diameter of 7 cm and the wall thickness of 2.5 cm (a schematic diagram of the die is shown in Fig. 3). Six horizontal channels (diameter: 2.7 mm) in the walls were used for the ignition wires, thermocouples, and removal of gases that may form during combustion. The pellet was installed inside this die and the igniter (a tungsten wire, folded in a waffle pattern and connected to the power supply) was located at the bottom of the

pellet. Silica powder was used as a pressure-transmitting medium. This powder (150 g) was poured into the die to fully surround the pellet. The die was placed under the aforementioned hydraulic press. Once ignition was achieved, the power supply was turned off. A jet of silica escaping from the apparatus through one of the horizontal channels indicated that combustion was occurring. Immediately after the end of combustion, the press was operated (force: 60−80 kN). After natural cooling of the die for about one hour, the obtained product pellet was removed. A thin layer of silica, adhered to the pellet surface, was removed using grinding paper.

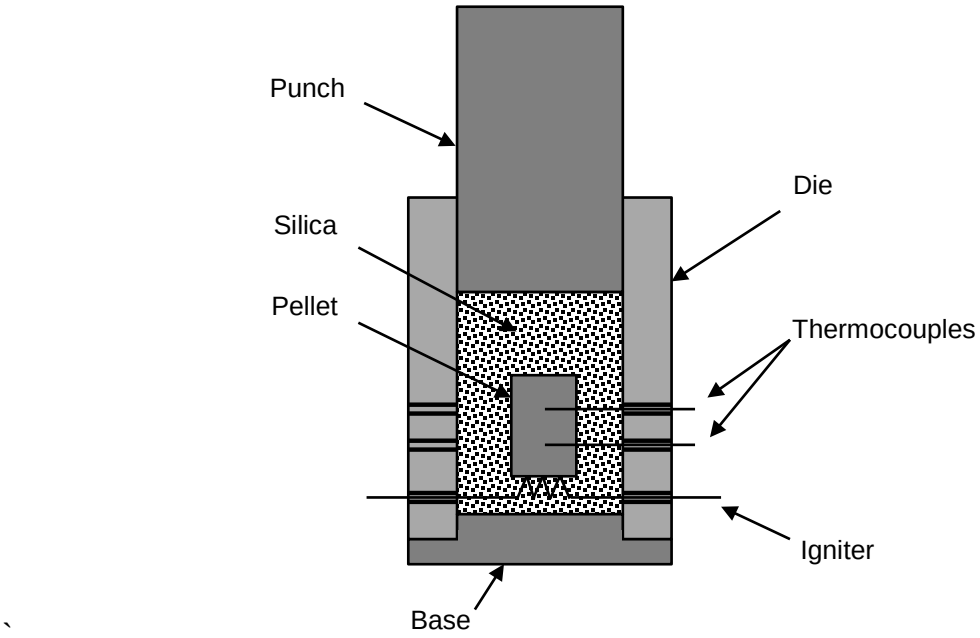


**Fig. 3. Schematic diagram of the die for SHS compaction.**

Chromel−Alumel thermocouples (type K, wire diameter: 250 μm, Omega Engineering) and WRe26%/WRe5% thermocouples (type C, wire diameter: 76 μm, Omega Engineering) were used to measure the temperature in the middle of the sample during the combustion process. The thermocouples, located in two-channel ceramic insulators, were inserted into pellets through drilled channels. The thermocouples were connected to a USB-based data acquisition system (National Instruments USB-9211).

A high-speed video camera (Vision Research Phantom v1210), equipped with a lens for macro shooting (Nikon AF Micro NIKKOR 60mm f/2.8D), was used for observations of the combustion process through a glass window. In the present research, the resolution was 1024x768 and the frame rate was 500 fps.

The as-milled powders and combustion products were analyzed using X-ray diffraction (Bruker D8 Discover XRD) and scanning electron microscopy (SEM, Hitachi S-4800).

Oxidation resistance of the obtained materials was studied using a thermogravimetric analyzer (Netzsch TGA 209 F1 Iris) and a differential scanning calorimeter (Netzsch DSC 404 F1 Pegasus). The TGA and DSC instruments were calibrated following manufacturer recommendations.

The compressive strength of the obtained materials was measured using a fatigue testing machine (INSTRON 8801) in accordance with ASTM standard C773. The elastic modulus and hardness were determined using a nanomechanical test instrument (Hysitron TI 750H Ubi).

## 2.2. Results and Discussions

### *2.2.1. Synthesis and characterization of $MoSi_2$-$Mo_5Si_3$ composites*

In the experiments conducted in an argon environment, it was possible to ignite 12.7-mm-diameter pellets without mechanical activation. The experiments, however, revealed a remarkable effect of mechanical activation on the velocity of the combustion front propagation: it increased from 2 mm/s to about 13 mm/s.

Figure 4 shows an XRD pattern of the as-milled powder. It is seen that the as-milled powder consists of Mo and Si. As there was no formation of $MoSi_2$ or $Mo_5Si_3$, it can be concluded that no reaction occurred during milling. XRD pattern of the combustion product (Fig. 5) shows that $MoSi_2$ is the major phase and $Mo_5Si_3$ is the secondary phase of the composite. No unreacted molybdenum or silicon was detected.

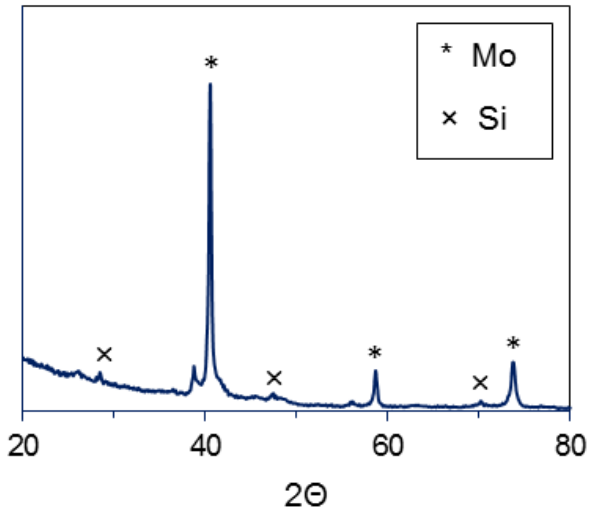


**Fig. 4. XRD pattern of as-milled Mo−Si powder.**

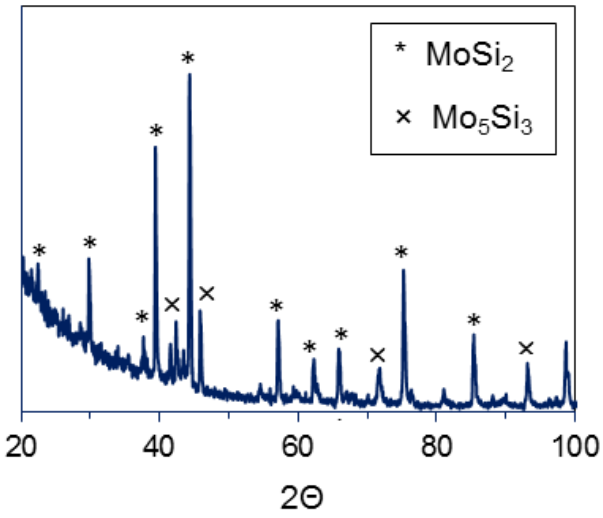


**Fig. 5. XRD pattern of products obtained by combustion of Mo−Si mixture.**

Measurements with the particle size analyzer have shown that before milling molybdenum has the volume mean diameter of 16.64 μm and median diameter of 11.25 μm, while silicon has the volume mean diameter of 10.15 μm and median diameter of 7.72 μm. Figure 6 shows the SEM images of Mo/Si mixture before and after milling as well an image of the combustion products. The image analysis indicates that milling decreased the particle size from about 10 μm to the submicron range (200−500 nm). Based on the SEM observations, it can be concluded that the structure of the as-milled powder may be considered as aggregates composed of molybdenum and silicon nanocrystals. This nanostructured Mo−Si material is easily ignited during SHS process. From the SEM image of the combustion products, it is seen that most particles have a size of 0.5−1 μm; they are agglomerated and form a three-dimensional network structure.

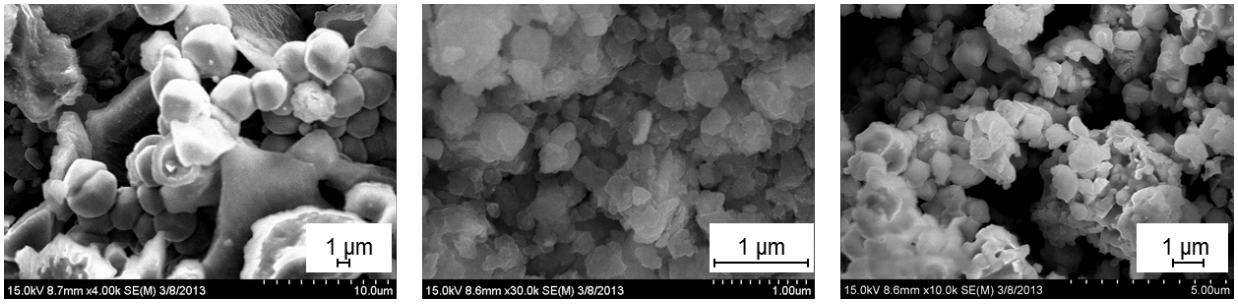


**Fig. 6. SEM micrographs of Mo−Si mixture (left) before milling, (middle) after milling, and (right) after combustion.**

The product obtained after SHS compaction had a low porosity and was significantly denser than that obtained after combustion in argon. Specifically, SHS compaction products exhibited an increase in density of 55−60% as compared to non-compacted products. The volume decreased due to decreasing the length, while the diameter remained almost the same as before the compaction. The XRD pattern obtained after SHS compaction was similar to that obtained by combustion in argon.

The SHS compaction product (diameter 25 mm; height 17 mm) was subjected to the compression test. The displacement rate of the top fixture was equal to 5 mm/min. During the test, when the load reached 37.9 kN, the product started to break (see the load-strain curve in Fig. 7). Based on the test results, compressive strength was determined to be 79 MPa.

Oxidation of the materials obtained by combustion in argon and by SHS compaction was studied using thermogravimetric analysis. The samples (mass: about 20 mg) in alumina crucibles (diameter: 5.85 mm) were heated in oxygen-argon (20% $O_2$) environment at a heating rate of 10 °C/min. The flow rates of oxygen and argon were 6 mL/min and 24 mL/min, respectively.

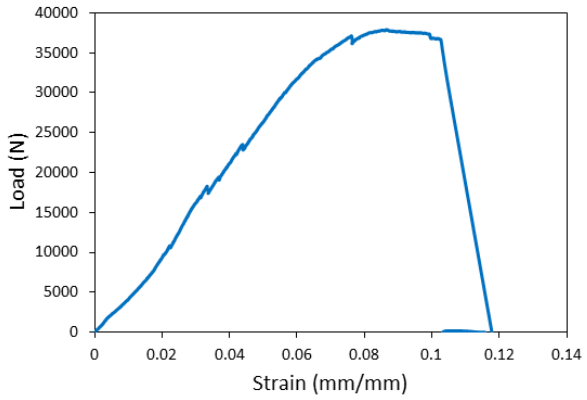


**Fig. 7. Load-strain curve obtained in the compression test.**

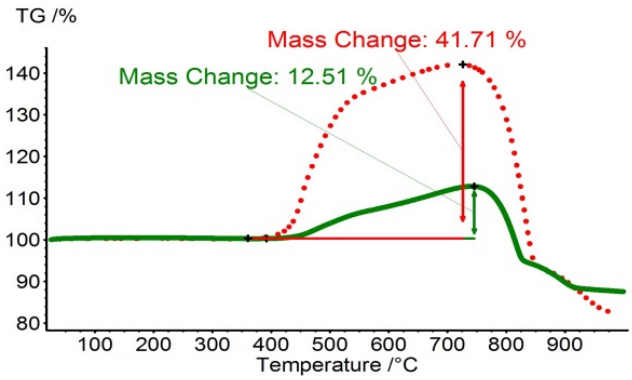


**Fig. 8. TG curves for the oxidation of $MoSi_2$–$Mo_5Si_3$ materials obtained by combustion in argon (dotted lines) and by SHS compaction (solid lines).**

Figure 8 shows the thermogravimtetric (TG) curves for the products obtained by combustion in argon and by SHS compaction. It is seen that qualitatively the two TG curves are similar. In both cases the mass increase, caused by oxidation, started at about 400 °C and reached the maximum at 720−750 °C. Further increase in the temperature led to dramatic loss of mass. Note that the mass loss during oxidation of Mo-rich silicides at temperatures over 700 °C is well known in the literature [1−5]; it is explained by volatilization of $MoO_3$ phase formed in the temperature range from 400 to 700 °C. Comparison of the two TG curves clearly shows that the use of SHS compaction significantly improves the oxidation resistance of $MoSi_2$–$Mo_5Si_3$ materials obtained by combustion synthesis. This effect is apparently associated with the lower porosity of SHS compaction products, which inhibits transport of oxygen to the inner surface of the obtained porous sample. It is expected that an increase in pressure during SHS compaction will further improve the oxidation resistance of the obtained $MoSi_2$–$Mo_5Si_3$ materials.

### *2.2.2. Synthesis and characterization of materials based on $Mo_5SiB_2$ phase*

The attempts to ignite (in argon) a mechanically activated mixture of Mo, Si, and B that corresponds to $Mo_5SiB_2$ phase were unsuccessful. To increase the exothermicity, the composition of the initial mixture was designed according to the stoichiometry of reactions that produce two phases: $Mo_5SiB_2$ and MoB. The idea of adding more boron is based on the higher exothermicity of Mo−B mixture: the adiabatic flame temperature of Mo−B equimolar mixture is equal to 2310 K (calculated at 1 atm using THERMO software [16]), i.e., by about 400 K higher than for Mo−Si (1:2 mole ratio) mixture. Table 1 shows the compositions of the prepared mixtures and of the expected products.

**Table 1. Compositions and combustion characteristics of the tested Mo−Si−B mixtures.**

| No. | Initial mixture | | | Expected product | | *u* | z | *f* | n | *v* | *u*·*z* |
|---|---|---|---|---|---|---|---|---|---|---|---|
| | **Mo** | **Si** | **B** | **$Mo_5SiB_2$** | **MoB** | | | | | | |
| | mol% | mol% | mol% | mol% | mol% | mm/s | mm | Hz | | mm/s | $mm^2/s$ |
| 1 | 62.5 | 12.5 | 25 | 100 | 0 | - | - | - | - | - | - |
| 2 | 62.16 | 12.16 | 25.68 | 90 | 10 | * | * | * | * | * | - |
| 3 | 61.76 | 11.76 | 26.47 | 80 | 20 | 2.5 | 0.94 | 2.6 | 1 | 121 | 2.4 |
| 4 | 61.13 | 11.13 | 27.74 | 67 | 33 | 2.9 | 0.85 | 3.4 | 3 | 47 | 2.5 |
| 5 | 60 | 10 | 30 | 50 | 50 | 3.6 | 0.73 | 4.9 | >3* | * | 2.6 |
| 6 | 59.09 | 9.09 | 31.82 | 40 | 60 | 4.1 | 0.64 | 6.3 | >3* | * | 2.6 |
| 7 | 58.29 | 8.29 | 33.42 | 33 | 67 | 5.6 | 0.56 | 10.0 | >3* | * | 3.1 |

* Accurate measurements were impossible in this case.

The combustion experiments were conducted with 12.7-mm-diameter pellets in an argon environment. The results confirmed that the proposed method for increasing the mixture exothermicity works: mixture #2 (see Table 1) ignited and the combustion front stopped before reaching the middle of the pellet, while for mixture #3, the front traveled 90% of the pellet height and for mixtures 4–7, the front reached the bottom of the pellet. All the pellets burned in the spin combustion regime where the combustion wave propagates as the motion of one or several hot spots along a helix on the pellet surface [17−21]. For mixture 3, initially one hot spot propagated (Fig. 9) and after passing the middle of the pellet height, a transition to the regime with two counter-propagating spots occurred. For mixture 4, the combustion started from two counter-propagating hot spots and after three cycles transformed into the so-called three-head spin where three hot spots are moving in the same direction along a helix (Fig. 10). For mixtures 5−7, the number of spots was larger and they were moving rapidly along the luminous zone boundary while this zone propagated toward the bottom end of the pellet. For all the samples, a distinct trace of the spinning front remained on the product surface.

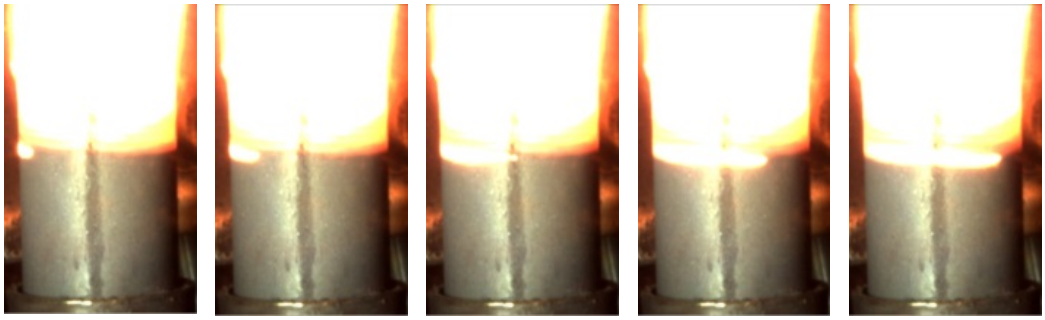


**Fig. 9. Propagation of a single spin over mixture #3 (Table 1) pellet. Time zero selected arbitrarily.**

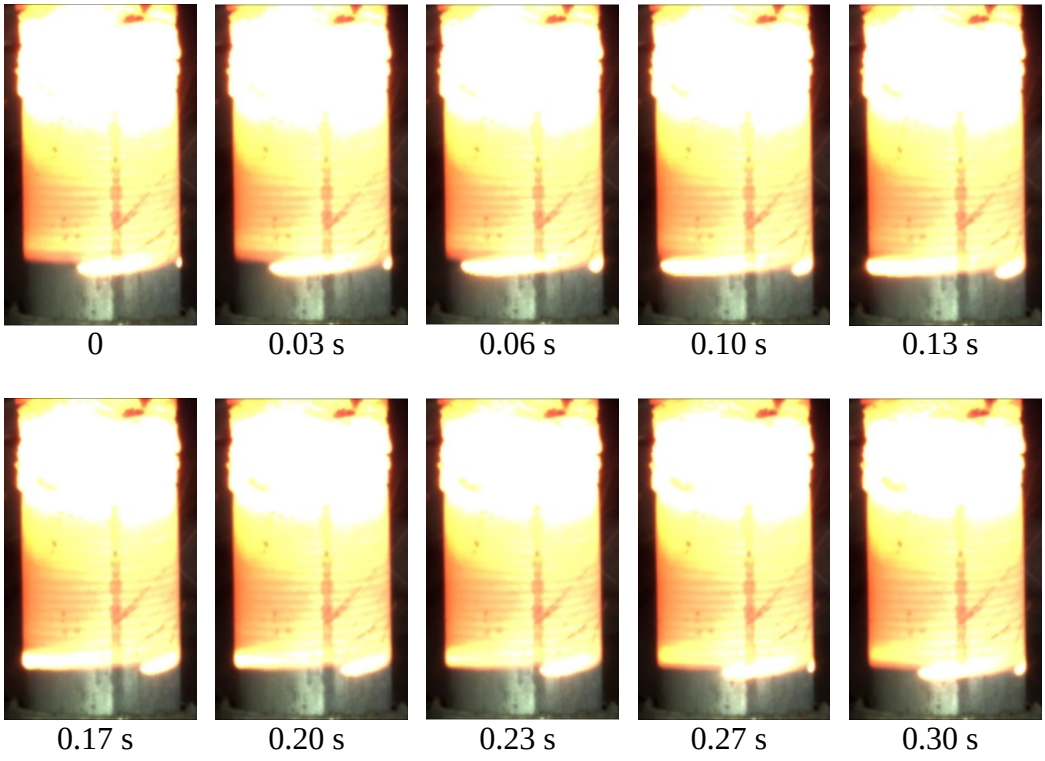


**Fig. 10. Propagation of a three-head spin over mixture #4 (Table 1) pellet. Time zero selected arbitrarily.**

The measured characteristics of the spinning front such as the axial velocity ($u$), pitch ($z$), frequency ($f$), number of spin heads ($n$), and tangential velocity ($v$), are shown in Table 1. The pitch and frequency were measured using the trace on the product surface. Note that one of the three characteristics $u$, $f$, and $z$ can also be calculated using the other two and an obvious relationship $u = f \cdot z$.

Different analytical and modeling approaches have been utilized to explain the spin combustion of solid systems [18−20]. A simplified theory of spin combustion developed by Novozhilov [18] predicts that the product $u \cdot z$ (or $u^2 \cdot f^{-1}$) is constant and of the same order of magnitude as the thermal diffusivity of the medium (the pitch plays a role of the preheat zone in the flame). The obtained values of $u \cdot z$ are, indeed, close to each other (see Table 1). It is also well known that for many powdered mixtures used in SHS, the thermal diffusivity is of the order of 1 $mm^2/s$ [22,23] so that the obtained values of $u \cdot z$ are of the same order of magnitude as the thermal diffusivity. In addition, the measured values of the tangential velocity $v$ for mixtures 3 and 4 (121 and 47 mm/s, respectively) correlate with the values 106 and 45 mm/s, respectively, obtained using the mass conservation equation: $v = \pi \cdot d \cdot u \cdot n^{-1} \cdot z^{-1}$, where $d$ is the pellet diameter. Thus, the obtained characteristics of spin combustion are in good agreement with Novozhilov's theory.

Thermocouple measurements have shown that in any of the tested Mo-Si-B mixtures the maximum temperature did not reach the melting point of Si, 1687 K (the melting points of Mo and B are much higher). Thus, the reaction mechanism during the observed spin combustion was based on solid-phase diffusion, with no liquid involved. Also, the temperature profiles contained a single maximum, indicating that the reactions occurred simultaneously.

X-ray diffraction analysis of the combustion products has shown that in each experiment, the obtained composition was not a binary ($Mo_5SiB_2$–MoB) mixture. Figure 11 shows an XRD pattern for mixture #4. The composition includes $Mo_5SiB_2$, MoB, $MoSi_2$, $Mo_5Si_3$, $Mo_2B$, and Mo. It is possible that the product also contains B, which cannot be seen in the pattern because amorphous boron was used in the experiments. It is seen that $Mo_5SiB_2$ and Mo exhibit the highest peaks and MoB is apparently the third major component. XRD patterns obtained for mixtures 5, 6, and 7 (Figs. 12-14) are similar, but they report an important trend: the Mo-to-$Mo_5SiB_2$ intensity ratio, determined using the highest peaks for each phase, is equal to 1.39, 1.18, 0.75, and 0.62 for mixtures 4, 5, 6, and 7, respectively. Thus, with increasing the content of MoB in the product composition, the content of Mo phase decreases.

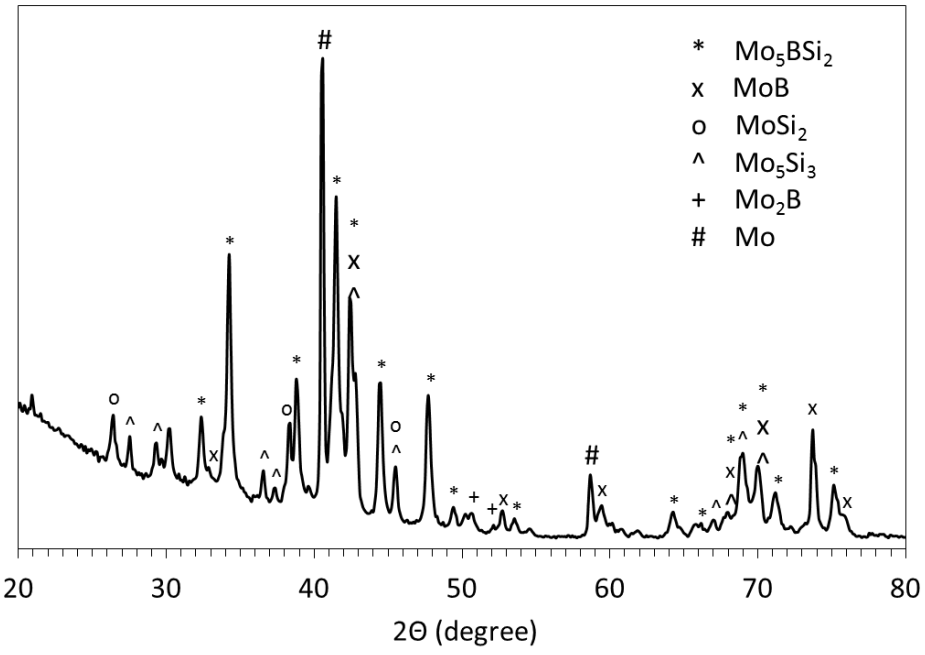


**Fig. 11. XRD pattern of products obtained by combustion of Mo−Si−B mixture #4 (Table 1).**

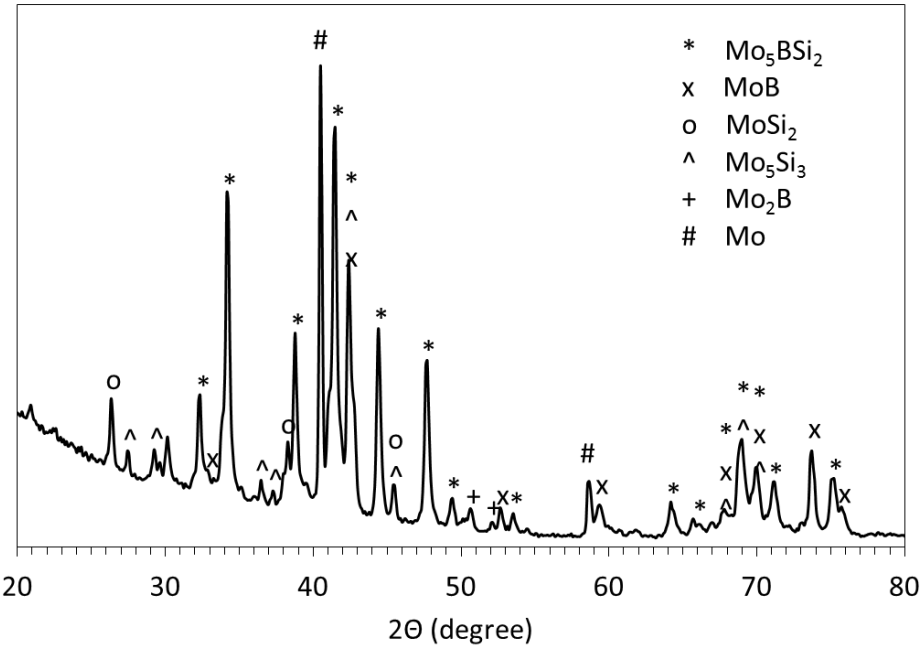


**Fig. 12. XRD pattern of products obtained by combustion of Mo−Si−B mixture #5 (Table 1).**

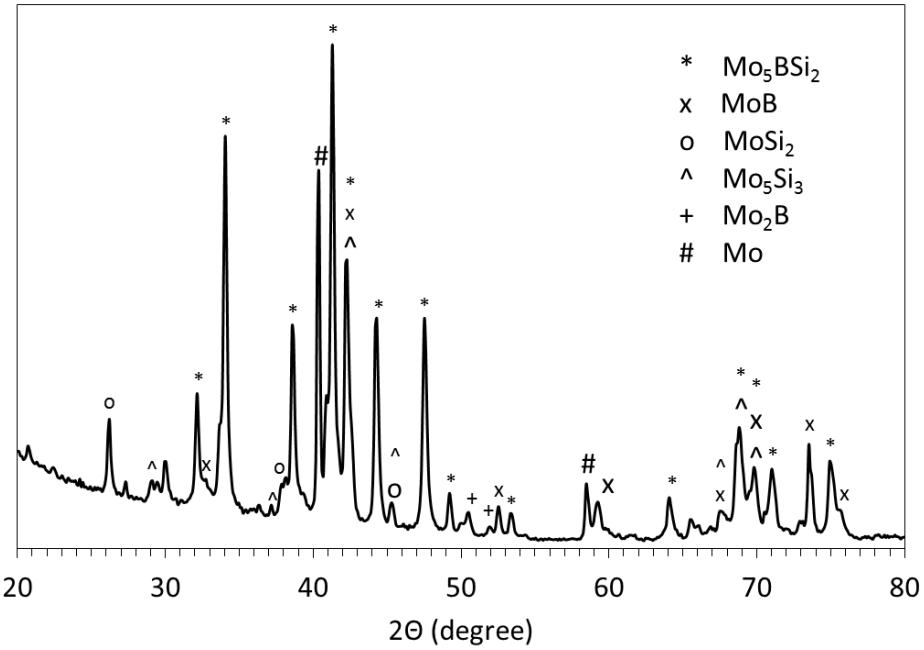


**Fig. 13. XRD pattern of products obtained by combustion of Mo−Si−B mixture #6 (Table 1).**

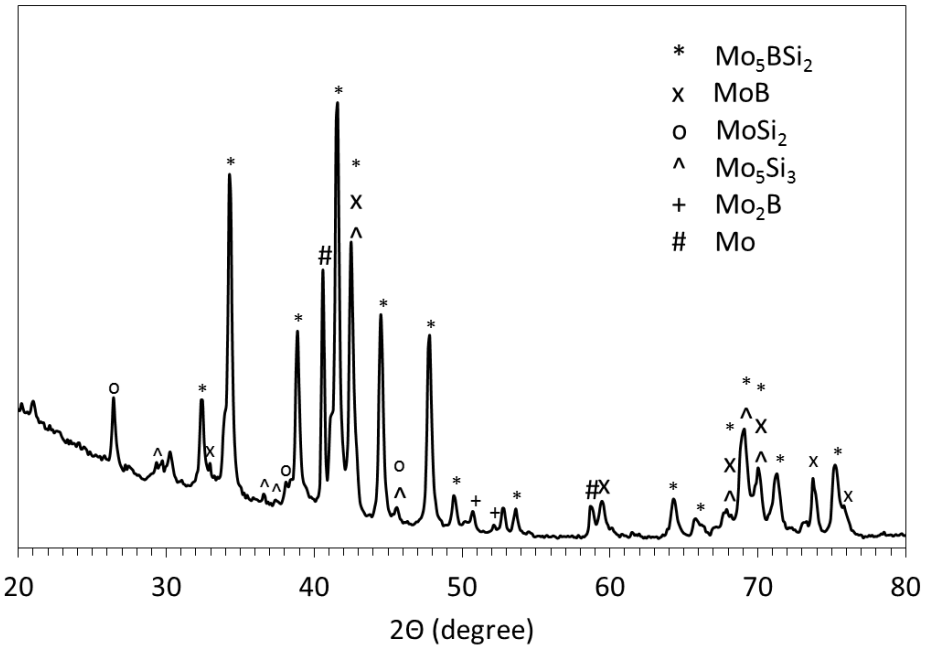


**Fig. 14. XRD pattern of products obtained by combustion of Mo−Si−B mixture #7 (Table 1).**

It is well known that increasing the amount of Mo phase improves mechanical properties of molybdenum silicides and borosilicides, but decreases the oxidation resistance because of the formation and volatilization of $MoO_3$ [1−5]. To determine the effect of Mo phase on the oxidation resistance of the obtained materials, mixtures 3, 4, and 7 were subjected to thermogravimetric analysis in oxygen−argon flow. The flow rate and the heating rate were the same as in the aforementioned tests of $MoSi_2$−$Mo_5Si_3$ composites. For all three samples, the TG and calculated differential thermal analysis (c-DTA) curves were virtually identical (Figs. 15-17). The mass increases are 54.5%, 54.8% and 54.2% for mixtures 3, 4, and 7, respectively. Thus, it can be concluded that oxidation resistance of the obtained Mo−Si−B materials is independent on the concentration of Mo phase in the products so that the materials with higher Mo contents are preferable because of better mechanical properties. The oxidation resistance of these materials could be improved by using SHS compaction as shown in Section 2.2.1.

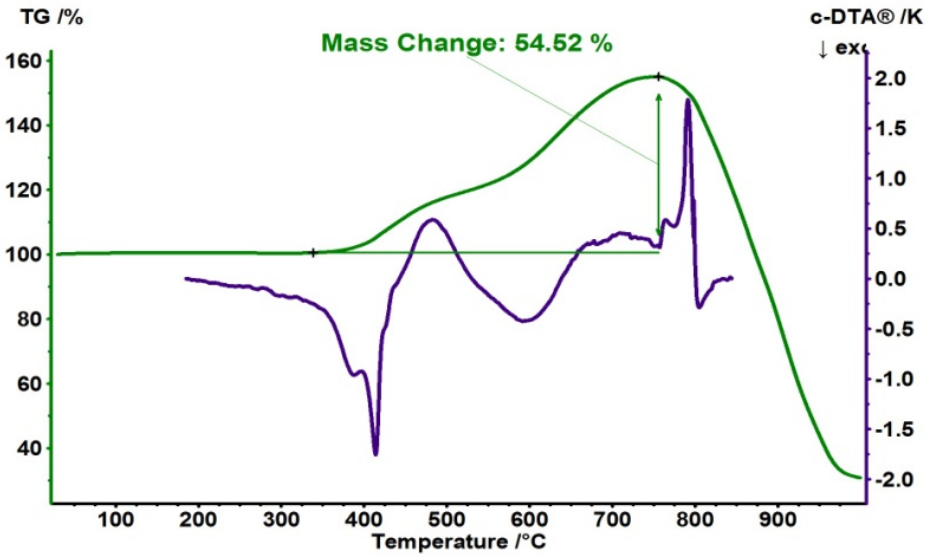


**Fig. 15. TG and c-DTA curves for the oxidation of the product obtained by combustion of Mo−Si−B mixture #3 (Table 1).**

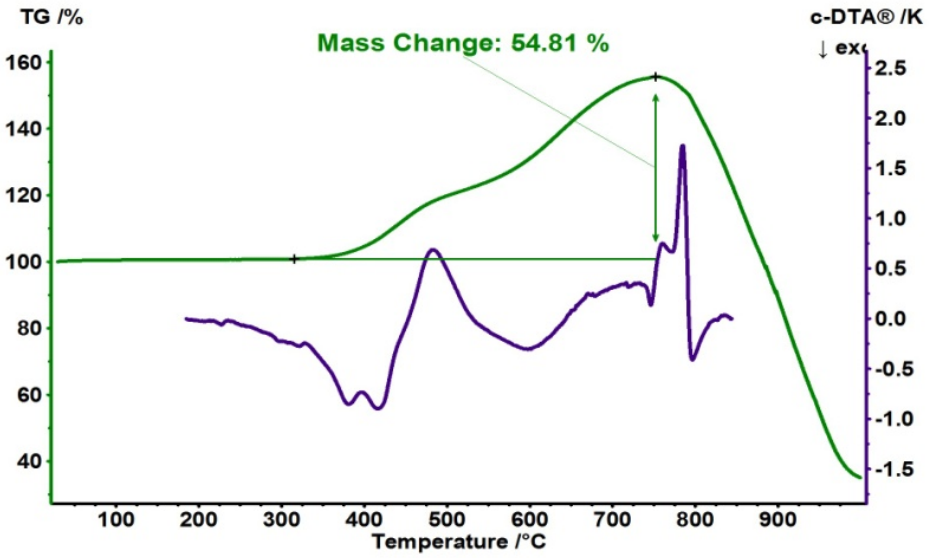


**Fig. 16. TG and c-DTA curves for the oxidation of the product obtained by combustion of Mo−Si−B mixture #4 (Table 1).**

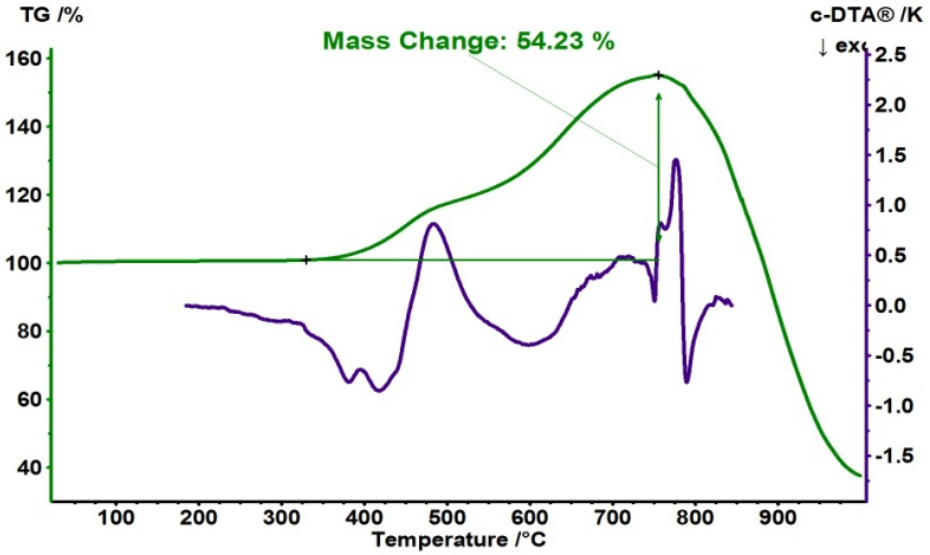


**Fig. 17. TG and c-DTA curves for the oxidation of the product obtained by combustion of Mo−Si−B mixture #7 (Table 1).**

### *2.2.3. Synthesis of $Mo_5SiB_2$–TiC, $Mo_5SiB_2$–$TiB_2$, and α-Mo–$Mo_5SiB_2$–$Mo_3Si$ materials*

Attempts to ignite Mo/Si/B/Ti/C mixtures, designed to obtain $Mo_5SiB_2$–TiC, using a booster pellet at the top were unsuccessful. In contrast, Mo/Si/B/Ti mixtures (for $Mo_5SiB_2$–$TiB_2$ materials) ignited successfully. In the mixture designed for 10 wt% $TiB_2$, however, the combustion front stopped at the middle of the pellet, while the mixtures with higher concentration of Ti/B additive burned entirely. Figure 18 shows the combustion propagation over the mixture designed for 15 wt% $TiB_2$. It is seen from the top series of images in Fig. 12 that the combustion front propagates downward with an approximately constant axial velocity (about 4 mm/s). The bottom series of images in Fig. 15 reveals a spinning structure of the combustion wave. Specifically, a counter-propagating motion is seen in the images with time labels 0.08 s and 0.1 s. This behavior of combustion wave propagation has been reported for the mixtures of JSC-1A lunar regolith simulant with magnesium [21] and obtained in numerical modeling of spin combustion [19, 20].

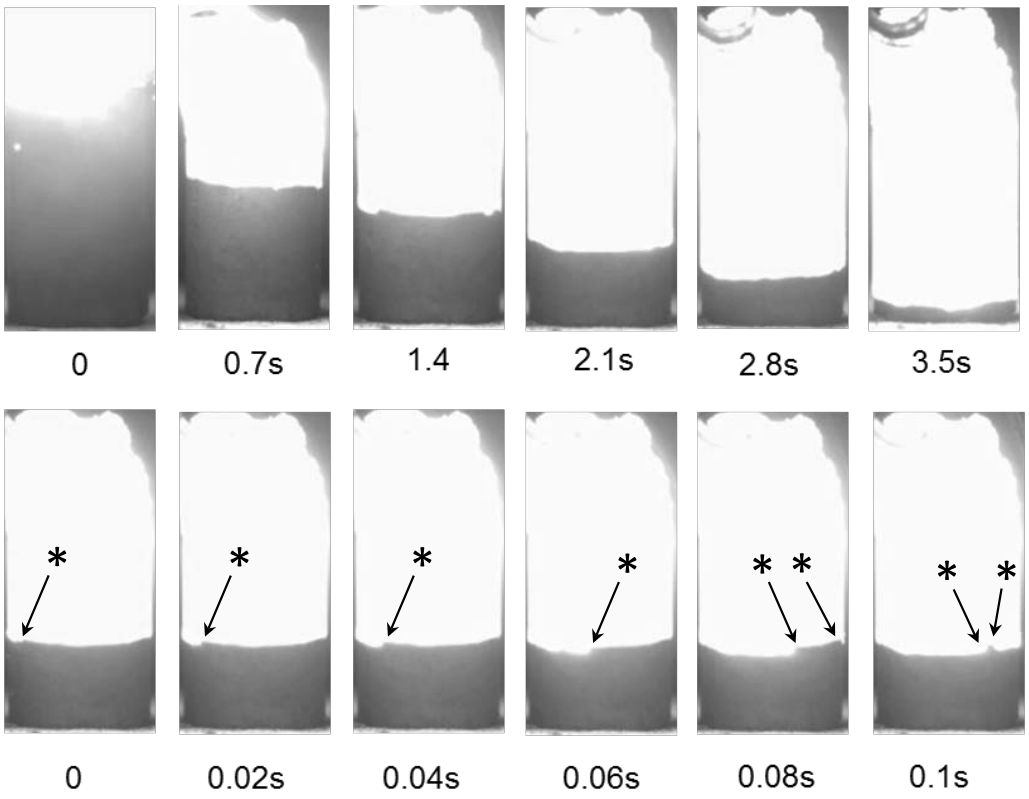


**Fig. 18. Combustion of Mo-Si-B-Ti mixture designed for 85% $Mo_5SiB_2$ and 15% $TiB_2$. The sample diameter was 13 mm. The top series of images shows the entire process, while the bottom one shows a fragment with shorter intervals between the images. In each series, time zero was selected arbitrarily. The first image in the top series shows combustion of the booster Ti/B layer. Asterisks show the leading edges of the spinning combustion wave.**

It is known that spin combustion occurs in low-exothermic mixtures, i.e. when the combustion temperature is low. Indeed, thermocouple measurements for this mixture have shown that the maximum temperature in the middle of the pellet was only about 1140 °C. Since the maximum temperature did not reach the melting point of Si, 1414 °C (the melting points of Mo and B are much higher), the reaction mechanism during the observed spin combustion was based on solid-phase diffusion, with no liquid involved. Also, the temperature profile contained a single maximum, indicating that the reactions occurred simultaneously.

Figure 19 shows the XRD pattern of products formed after combustion of the mixture designed for 20 wt% $TiB_2$. It is seen that along with the desired $Mo_5SiB_2$ and $TiB_2$ phases, there are also significant peaks of Mo, MoB, and $Mo_5Si_3$.

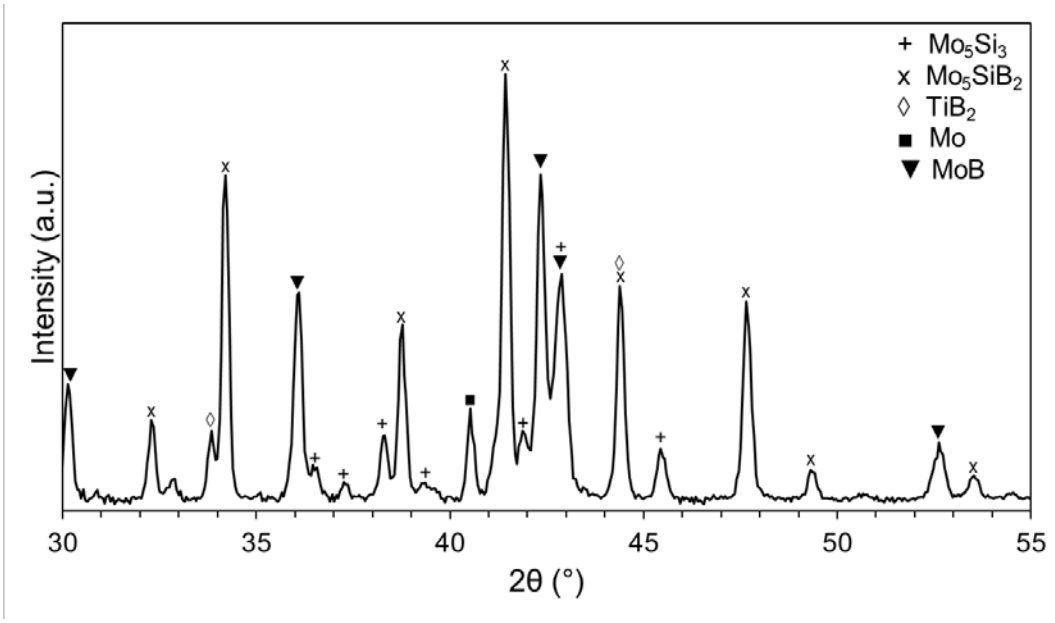


**Fig. 19. XRD patterns of products obtained by combustion (conventional SHS) of Mo/Si/B/Ti mixture designed for 80% $Mo_5SiB_2$ and 20% $TiB_2$.**

With increasing the concentration of Ti/B additive, the peak of Mo decreases, but the intensities of MoB peaks increase. For example, Figure 20 shows that in the products formed after combustion of the mixture designed for 40 wt% $TiB_2$, there is no Mo peak, but MoB becomes the dominant phase.

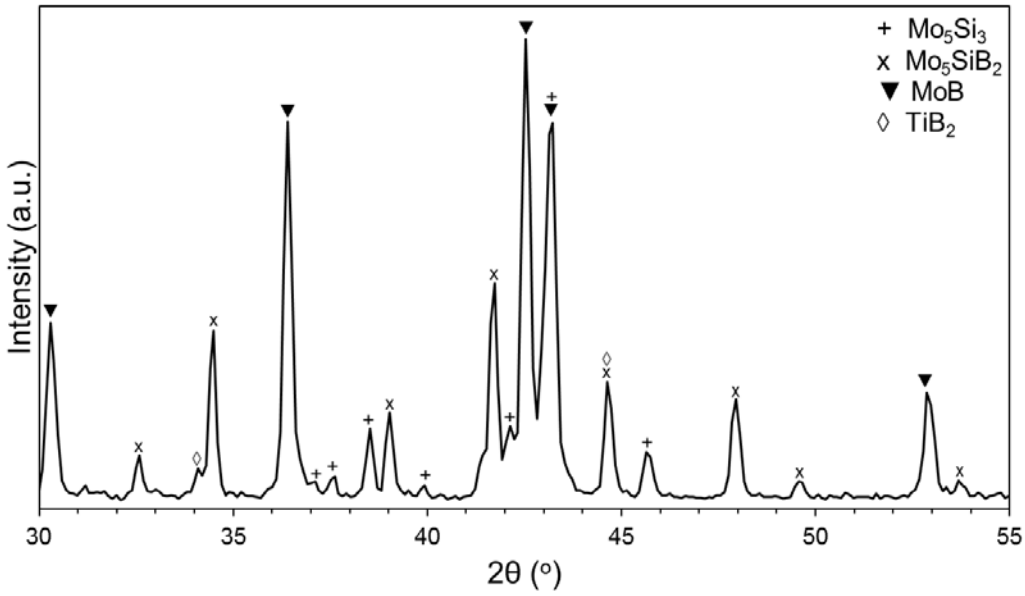


**Fig. 20. XRD patterns of products obtained by combustion (conventional SHS) of Mo/Si/B/Ti mixture designed for 60% $Mo_5SiB_2$ and 40% $TiB_2$.**

These results lead to the conclusion that it is impossible to obtain desired two-phase $Mo_5SiB_2$–TiC and $Mo_5SiB_2$–$TiB_2$ materials by a conventional SHS with ignition at the top of the pellet. For this reason, it was decided to focus on the use of the chemical oven technique. This has enabled successful ignition and combustion of Mo/Si/B/Ti/C mixtures. Figure 21 shows the XRD pattern of the products obtained by combustion of Mo/Si/B/Ti/C mixture designed for 15 wt% TiC. It is seen that $Mo_5SiB_2$ phase dominates, while MoB peaks are relatively small and there are no peaks of Mo and $Mo_5Si_3$.

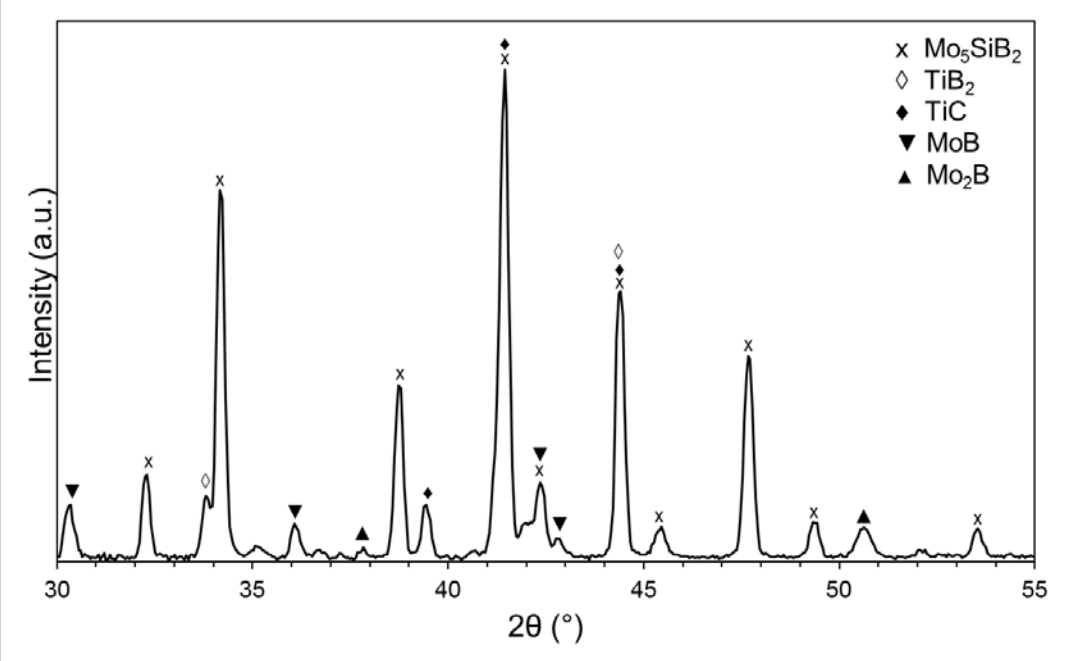


**Fig. 21. XRD pattern of products obtained by combustion (chemical oven) of Mo/Si/B/Ti/C mixture designed for 85% $Mo_5SiB_2$ and 15% TiC.**

The use of the chemical oven technique has also led to a better quality of products obtained by combustion of Mo/Si/B/Ti mixtures designed for the fabrication of $Mo_5SiB_2$–$TiB_2$ materials. Figure 22 shows the XRD pattern of the products obtained by combustion of Mo/Si/B/Ti mixture designed for 15 wt% $TiB_2$. It is seen that MoB peaks are relatively small and there are no peaks of Mo and $Mo_5Si_3$.

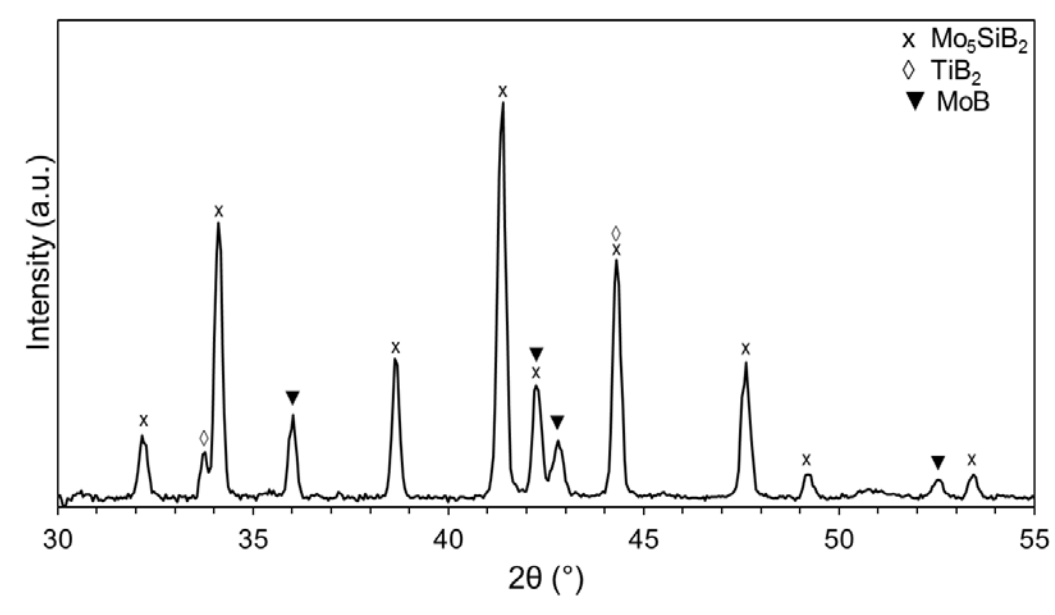


**Fig. 22. XRD pattern of products obtained by combustion (chemical oven) of Mo/Si/B/Ti mixture designed for 85% $Mo_5SiB_2$ and 15% $TiB_2$.**

The lower concentrations of secondary phases in the products obtained by the chemical oven technique are likely associated with the higher temperatures during combustion. Indeed, the temperatures measured during these experiments were as high as about 3000 °C, i.e. close to the adiabatic flame temperature of the stoichiometric Ti/B mixture used as the shell. At such high temperatures, all reactants were molten and the reactions were fast, resulting in better conversion to thermodynamically expected products and in the formation of low-porous materials.

For all mixtures, conventional SHS process led to the formation of a porous product with cracks. In contrast, the experiments conducted with the chemical oven technique have produced low-porous materials, with no cracks except for the ends of the pellet. For illustration, Figure 23 shows products obtained after combustion of the same mixture in a conventional SHS mode and using the chemical oven technique. The top part of the left pellet is the product of the booster layer combustion (i.e. $TiB_2$), while the right pellet is shown after removing the shell of booster mixture products.

**Fig. 23. Combustion products of Mo/Si/B/Ti mixture designed for 85% $Mo_5SiB_2$ and 15% $TiB_2$. The left pellet was obtained by conventional SHS, while the right product was obtained by the chemical oven technique.**

The elastic modulus and hardness at room temperature were determined for $Mo_5SiB_2$–TiC and $Mo_5SiB_2$–$TiB_2$ materials obtained by the chemical oven technique. These characteristics are 109 GPa and 1.24 GPa, respectively, for $Mo_5SiB_2$–TiC material. The obtained $Mo_5SiB_2/TiB_2$ material has better elastic modulus and hardness: 135 GPa and 2.40 GPa, respectively. The density of this material is 7.7 g/cm$^3$.

The chemical oven technique has also enabled combustion synthesis of α-Mo–$Mo_5SiB_2$–$Mo_3Si$ materials. Figure 24 shows a typical XRD pattern of the material obtained from Mo/12Si/8.5B mixture**.** The peaks correspond to the desired α-Mo, $Mo_5SiB_2$, and $Mo_3Si$ phases, with no other phases detected. Considering the highest peak for each phase, $Mo/Mo_3Si/Mo_5SiB_2$ intensity ratio is 3.7 : 1.3 : 1. Since the highest peaks of the three phases are close to each other and partly overlap, the intensity ratio was estimated based on the peak heights only. Although accurate quantitative analysis of XRD results was not conducted, it is seen that Mo dominates in the XRD pattern and the highest peak of $Mo_3Si$ exceeds the highest peak of $Mo_5SiB_2$. This is in agreement with the ratio of phase contents in the desired Mo–12Si–8.5B material, where $Mo/Mo_3Si/Mo_5SiB_2$ mole and mass ratios are 8.23 : 1.82 : 1 and 9.55 : 1.86 : 1, respectively (here the densities of the three phases were assumed to be 10.22, 8.97, and 8.81 g/cm$^3$, respectively [7]).

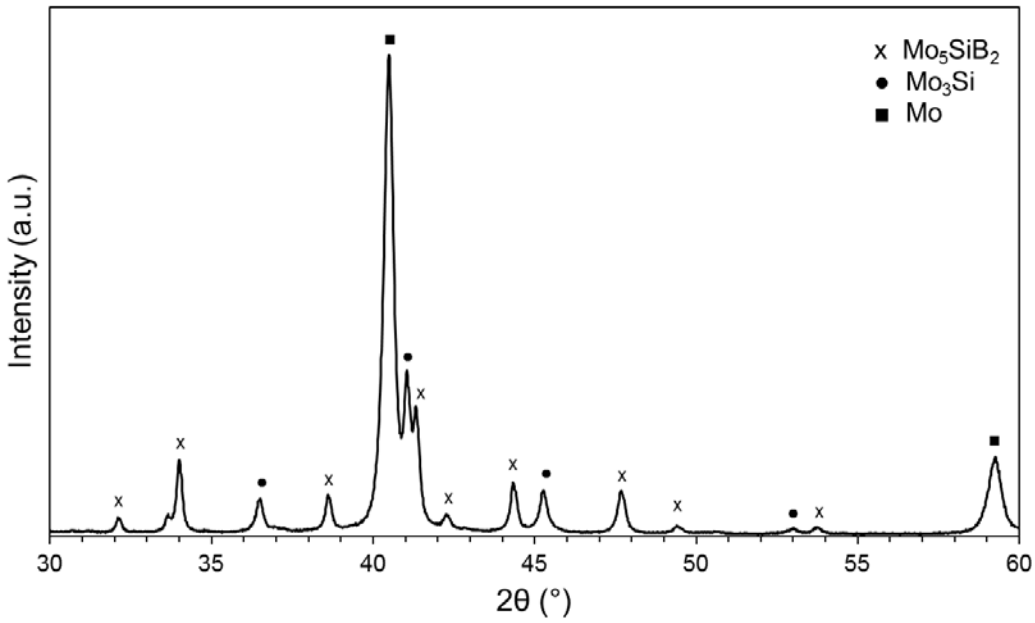


**Fig. 24. XRD pattern of products obtained by combustion of Mo/12Si/8.5B mixture.**

The compressive strength of Mo−12Si−8.5B alloy synthesized by the chemical oven technique was as high as 524 MPa (Fig. 25), while the density was in the range of 7.0−7.6 g/cm$^3$. Note that molybdenum possesses a compressive strength of 400 MPa [24] and has a density of 10.2 g/cm$^3$, i.e. the obtained materials are stronger and lighter than molybdenum. To our knowledge, there are no data on compressive strength of Mo−12Si−8.5B alloys prepared by arc melting in the literature, but it has been reported that these materials have a flexural strength of 539 MPa at room temperature [7]. Apparently, Mo-12Si-8.5B materials obtained by chemical oven and arc melting have a similar strength.

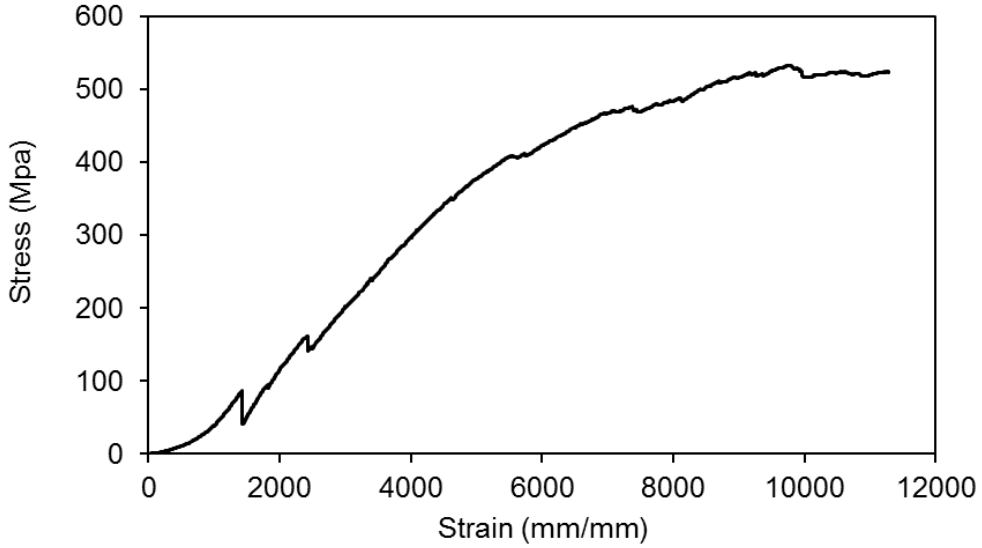


**Fig. 25. Stress-strain curve for the obtained Mo−12Si−8.5B alloy.**

### *2.2.4. Oxidation of $Mo_5SiB_2$–TiC, $Mo_5SiB_2$–$TiB_2$, and α-Mo–$Mo_5SiB_2$–$Mo_3Si$ materials*

Figure 26 shows thermogravimetric curves obtained for the obtained materials heated in oxygen/argon (20% $O_2$ / 80% Ar) gas flow to a temperature of 1000 °C, the maximum operating temperature of the used TGA instrument. Alumina crucibles were used, the gas flow rate was 30 mL/min, and the heating rate was 10 °C/min in all runs.

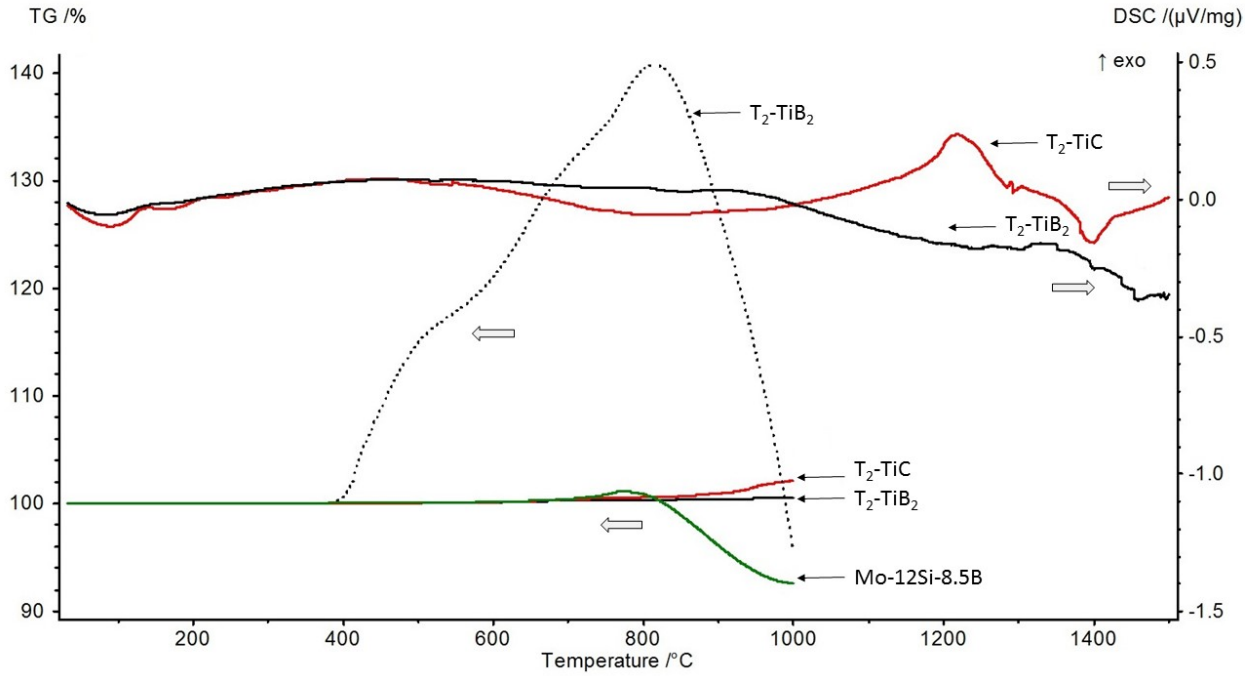


**Fig. 26. TGA and DSC of the materials obtained by conventional SHS (dotted curve) and by the chemical oven technique (solid curves).**

It is seen that oxidation of $Mo_5SiB_2$–$TiB_2$ material obtained by conventional SHS starts at about 400 °C. The sample exhibited a mass gain of about 40 % at 800 °C, followed by a catastrophic loss of mass.

$Mo_5SiB_2$–$TiB_2$ materials obtained by the chemical oven technique are much more resistant to oxidation. The mass gain is about 0.3 % at 700 °C. The TG curve has a plateau at 700−800 °C. With increasing the temperature to 1000 °C, the mass gain increases to about 0.5 %. For $Mo_5SiB_2$–TiC material, the mass gain at 700 °C is about 0.4 %, but further heating leads to a mass gain of about 2 % at 1000 °C.

TG curves for Mo−12Si−8.5B alloys show that they are more prone to oxidation than $Mo_5SiB_2$–$TiB_2$ and $Mo_5SiB_2$–TiC materials (when all the materials were obtained by the chemical oven technique): the mass gain at 700−800 °C is larger and the loss of mass at 1000 °C is significant.
Since the TGA has shown that $Mo_5SiB_2$–$TiB_2$ and $Mo_5SiB_2$–TiC materials obtained by the chemical oven technique exhibit the best oxidation resistance over the tested range of

temperatures, their oxidation was also studied using the DSC instrument that allows tests to be performed over a wider range of temperatures, up to 1500 °C. The DSC tests were conducted at the same gas flow rate and heating rate as in the TGA tests.

The DSC curve for $Mo_5SiB_2$–TiC material has a distinct exothermic peak with the maximum at about 1200 °C. The onset of the peak is at about 800 °C, which correlates with the TG curve for this material. There exists also an endothermic peak with the maximum at about 1400 °C, which indicates endothermic phase transformation. In contrast, the DSC curve for $Mo_5SiB_2$–$TiB_2$ material has a less distinct exothermic peak with the maximum at about 1320 °C and also a less distinct endothermic peak with the maximum at about 1450 °C.

Figures 27 and 28 show XRD patterns of $Mo_5SiB_2$–TiC and $Mo_5SiB_2$–$TiB_2$ materials obtained by the chemical oven technique and heated to 1500 °C in $O_2$/Ar flow. Comparison of these patterns with those in Figs. 21 and 22, respectively, shows that the oxidation led to the appearance of Mo phase and small peaks of $Mo_2B$ in both materials. This may be associated with the formation of protective borosilicate coating. Indeed, if this coating forms, part of molybdenum is released from $T_2$ phase, thus leading to the appearance of the aforementioned phases. The endothermic peaks in DSC curves (Fig. 26) may also be associated with the formation of these phases.

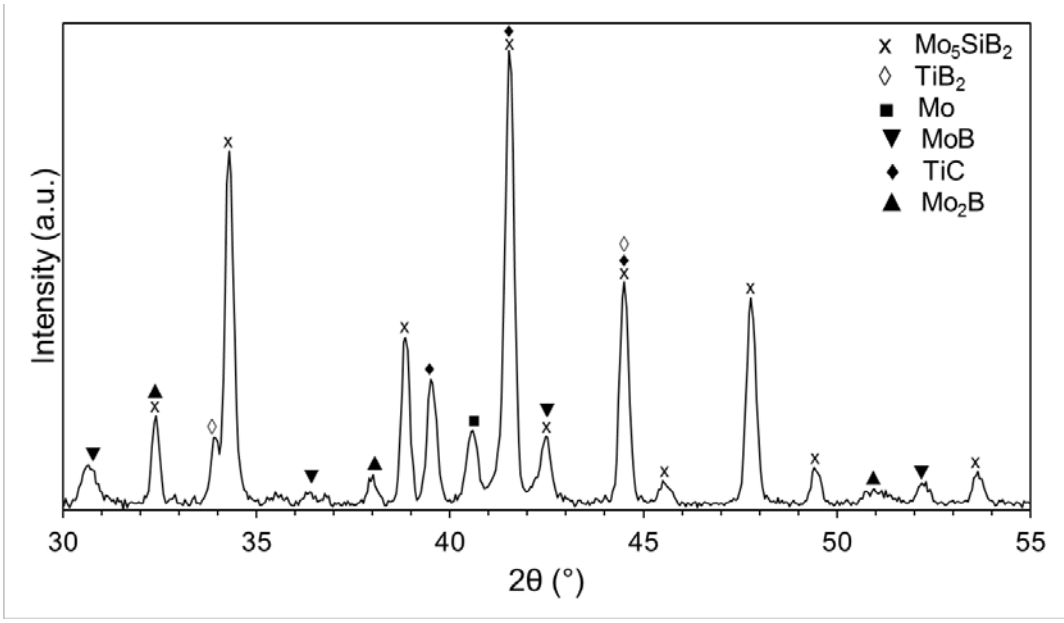


**Fig. 27. XRD pattern of $Mo_5SiB_2$–TiC material obtained by the chemical oven technique and heated to 1500 °C in $O_2$/Ar flow.**

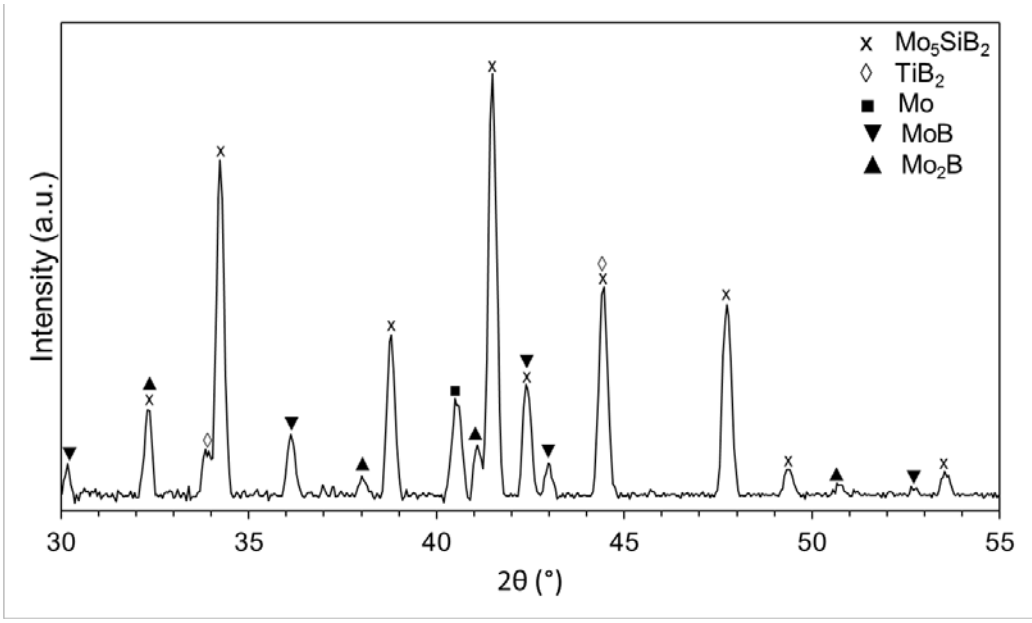


**Fig. 28. XRD pattern of $Mo_5SiB_2$–$TiB_2$ material obtained by the chemical oven technique and heated to 1500 °C in $O_2$/Ar flow.**

In summary, the TGA and DSC results as well as XRD analysis of heated samples indicate that $Mo_5SiB_2/TiB_2$ material obtained by the chemical oven technique has excellent oxidation resistance at temperatures up to 1500 °C. Its oxidation resistance is also better than for any other material obtained in the present work.

## 2.3. Conclusion

$MoSi_2$−$Mo_5Si_3$ composites and several materials based on $Mo_5SiB_2$ phase have been obtained by mechanically activated combustion synthesis conducted in a conventional SHS mode and using the chemical oven technique. It has been shown that use of SHS compaction (quasi-isostatic pressing) significantly improves oxidation resistance of the obtained $MoSi_2$−$Mo_5Si_3$ composites.

Combustion of Mo−Si−B mixtures for the formation of $Mo_5SiB_2$ phase becomes possible if the composition is designed for the addition of reactions leading to the formation of molybdenum boride. These mixtures exhibit spin combustion, the characteristics of which are in good agreement with the spin combustion theory. Oxidation resistance of the obtained Mo−Si−B materials is independent on the concentration of Mo phase in the products so that the materials with a higher Mo content are preferable because of better mechanical properties.

Pellets of Mo/Si/B/Ti mixtures, the composition of which corresponded to the formation of two-phase $Mo_5SiB_2$–$TiB_2$ product (10 – 40 wt% $TiB_2$), exhibited a self-sustained propagation of a spinning combustion wave upon ignition at the top. The products were porous and contained secondary phases such as $Mo_5Si_3$, MoB, and Mo in addition to the desired $Mo_5SiB_2$ and $TiB_2$, which is explained by relatively low combustion temperatures. During TGA test in $O_2$/Ar flow,

the obtained materials exhibited a mass gain of about 40 % at 800 °C, followed by a catastrophic loss of mass.

The chemical oven technique, involving combustion of a highly exothermic Ti/B mixture shell, has enabled fabrication of dense $Mo_5SiB_2$-based materials with TiC and $TiB_2$ additives as well as synthesis of α-Mo–$Mo_5SiB_2$–$Mo_3Si$ (Mo–12Si–8.5B) alloy. The products had low contents of secondary phases and low porosities as compared with $Mo_5SiB_2$–$TiB_2$ materials obtained by conventional SHS. The Mo–12Si–8.5B material was stronger and lighter than molybdenum. During TGA test in $O_2$/Ar flow, however, it lost several percent of mass at 1000 °C. The oxidation resistance of $Mo_5SiB_2$–TiC and $Mo_5SiB_2$–$TiB_2$ materials obtained by the chemical oven technique was much better. The latter was especially resistant to the oxidation at temperatures up to 1500 °C (the maximum temperature in the test) and also had higher elastic modulus and hardness than the former.

*In summary, the research has shown that mechanically activated combustion synthesis can be successfully used for the fabrication of $MoSi_2$–$Mo_5Si_3$ composites and materials based on $Mo_5SiB_2$ phase. For the first time, $Mo_5SiB_2$–$TiB_2$ material has been synthesized. This material, obtained by the chemical oven technique, has good mechanical properties and excellent oxidation resistance at temperatures up to 1500 °C.*

## 3. References


1. J.H. Perepezko, The hotter the engine, the better, Sci. 326 (2009) 1068–1069.
2. D.M. Dimiduk, J.H. Perepezko, Mo-Si-B Alloys: Developing a revolutionary turbine-engine material, MRS Bull. 28 (2003) 639−645.
3. J.H. Perepezko, R. Sakidja, K.S. Kumar, in: W. Soboyejo (Ed.), Mo-Si-B Alloys for ultrahigh temperature applications, Advanced Structural Material CRC Press, Boca Raton, (2007).
4. J.A. Lember, R.O. Ritchie, Mo-Si-B alloys for ultrahigh-temperature structural applications, Adv. Mater. 24 (2012) 3445–3480.
5. R. Mitra, Mechanical behavior and oxidation resistance of structural silicides, Int. Mater. Rev. 51 (2006) 13−60.
6. M. Akinc, M.K. Meyer, M.J. Kramer, A.J. Thom, J.J. Huebsch, B. Cook, Boron-doped molybdenum silicides for structural applications, Intermet. A 261 (1999) 16–23.
7. J.H. Schneibel, M.J. Kramer, O. Unal, R.N. Wright, Processing and mechanical properties of a molybdenum silicide with the composition Mo-12Si-8.5B (at.%), Intermet. 9 (2001) 25−31.
8. H. Choe, D. Chen, J.H. Schneibel, R.O. Ritchie, Ambient to high temperature fracture toughness and fatigue-crack propagation behavior in a Mo-12Si-8.5B (at.%) intermetallic, Intermet. 9 (2001) 319−329.
9. M. Kruger, S. Franz, H. Saage, M. Heilmaier, J.H. Schneibel, P. Jehanno, M. Boning, H. Kestler, Mechanically alloyed Mo-Si-B alloys with a continuous α-Mo matrix and improved mechanical properties, Intermet. 16 (2008) 933–941.
10. S. Miyamoto, K. Yoshimi, S.-H. Ha, T. Kaneko, J. Nakamura, T. Sato, K. Maruyama, R. Tu, T. Goto, Metall. Phase equilibria, microstructure, and high-temperature strength of TiC-added Mo-Si-B alloys, Mater. Trans. A 45A (2014) 1112−1123.
11. K. Yoshimi, J. Nakamura, D. Kanekon, S. Yamamoto, K. Maruyama, H. Katsui, T. Goto, High-temperature compressive properties of TiC-added Mo-Si-B alloys, JOM 66 (2014) 1930−1938.
12. A. Yamauchi, K. Yoshimi, K. Kurokawa, S. Hanada, Synthesis of Mo-Si-B in situ composites by mechanical alloying, J. Alloy. Compd. 434–435 (2007) 420–423.
13. P. Jehanno, M. Heilmaier, H. Saage, M. Boning, H. Kestler, J. Freudenberger, S. Drawin, Assessment of the high temperature deformation behavior of molybdenum silicide alloys, Mater. Sci Eng. A 463 (2007) 216–223.
14. C. Gras, E. Gaffet, F. Bernard, Combustion wave structure during the $MoSi_2$ synthesis by mechanically-activated self-propagating high-temperature synthesis (MASHS): In situ time-resolved investigations, Intermet. 14 (2006) 521–529.
15. M.A. Korchagin, D.V. Dudina, Application of self-propagating high-temperature synthesis and mechanical activation for obtaining nanocomposites, Combust. Explos. Shock Waves 43 (2007) 176–187.

16. A.A. Shiryaev, Thermodynamics of SHS processes: Advanced approach, Int. J. SHS 4 (1995) 351−362

17. A.G. Merzhanov, A.K. Filonenko, I.P. Borovinskaya, New phenomena in combustion of condensed systems, Sov. Phys. Dokl. 208 (1973) 122–125.

18. B.V. Nonozhilov, The theory of surface spin combustion, Pure Appl. Chem. 65 (1993) 309−316.

19. A. Bayliss, B.J. Matkowsky, A.P. Aldushin, Dynamics of hot spots in solid fuel combustion, Phys. D 166 (2002) 104–130.

20. T.P. Ivleva, A.G. Merzhanov, Three-dimensional modes of unsteady solid-flame combustion, Chaos 13 (2003) 80−86.

21. F. Álvarez, C. White, A.K. Narayana Swamy, E. Shafirovich, Combustion wave propagation in mixtures of JSC-1A lunar regolith simulant with magnesium, Proc. Combust. Inst. 34 (2013) 2245–2252.

22. A.A. Zenin, A.G. Merzhanov, G.A. Nersisyan, Thermal wave structure (by the example of boride synthesis), Combust. Explo. Shock Waves 17 (1981) 63−71.

23. E.A. Butakova, A.G. Strunina, Thermophysical properties of some thermite and intermetallic systems, Combust. Explo. Shock Waves 21 (1985) 67−69.

24. ASM Handbook, Vol.2: Properties and Selection: Nonferrous Alloys and Special-Purpose Materials, 10th ed., ASM International, Materials Park, OH, 1990.

# 4. Bibliography


1. Esparza, A.E., and Shafirovich, E., "Mechanically Activated Combustion Synthesis of Molybdenum Borosilicides for Ultrahigh-Temperature Structural Applications," in preparation, *Journal of Alloys and Compounds*, under review.
2. Alam, M.S., Esparza, A.A., and Shafirovich, E., "Combustion Synthesis of Molybdenum Silicides and Borosilicides," *MRS Proceedings*, 2015, 1760, mrsf14-1760-yy03-02 doi:10.1557/opl.2014.964.
3. Alam, M.S., and Shafirovich, E., "Mechanically Activated Combustion Synthesis of Molybdenum Silicides and Borosilicides for Ultrahigh-Temperature Structural Applications," *Proceedings of the Combustion Institute*, Vol. 35, 2015, No. 2, pp. 2275-2281 doi: 10.1016/j.proci.2014.05.019.
4. Esparza, A.A., Alam, M.S., and Shafirovich, E., "Mechanically Activated SHS of Molybdenum Borosilicides for Ultrahigh-Temperature Structural Applications," 9th U.S. National Combustion Meeting, May 17-20, 2015, Cincinnati, OH, Paper 2B06.
5. Esparza, A.A., and Shafirovich, E., "Mechanically Activated SHS of Molybdenum Borosilicides for Ultrahigh-Temperature Structural Applications," 5th Southwest Energy Science and Engineering Symposium, El Paso, TX, April 4, 2015.
6. Alam, M.S., and Shafirovich, E., "Combustion Synthesis of Molybdenum Borosilicides for Ultrahigh-Temperature Structural Applications," 4th Southwest Energy Science and Engineering Symposium, El Paso, TX, March 22, 2014.
7. Alam, M.S., and Shafirovich, E., "Combustion Synthesis of Molybdenum Silicides and Borosilicides for Ultrahigh-Temperature Structural Applications," *Spring Technical Meeting of the Central States Section of the Combustion Institute, March 16-18, 2014, Tulsa, OK*, Paper B-601.
8. Alam, M.S., and Shafirovich, E., "Mechanically Activated SHS Compaction of Molybdenum Disilicide Based Composites," XII International Symposium on Self-Propagating High Temperature Synthesis, 21 - 24 October 2013, South Padre Island, TX, p. 92.
9. Alam, M.S., and Shafirovich, E., "Mechanically Activated SHS Compaction of $MoSi_2$-Based Composites," *8th U.S. National Combustion Meeting, May 19-22, 2013, Park City, UT*, Paper 070HE-0301.
10. Alam, M.S., and Shafirovich, E., "Combustion Synthesis and Densification of $MoSi_2$-$Mo_5Si_3$ Composites," 3rd Southwest Energy Science and Engineering Symposium, El Paso, TX, April 27, 2013.